Preparation, structural and hydrotreating catalytic properties of unsupported $NiRh_2S_4$

Hiroyuki Yasuda,†[a] Christophe Geantet,*[a] Pavel Afanasiev,[a] Mimoun Aouine,[a] Thierry Epicier[b] and Michel Vrinat[a]

[a] *Institut de Recherches sur la Catalyse, CNRS, 2, Avenue Albert Einstein, 69626 Villeurbanne cedex, France. E-mail: geantet@catalyse.univ-lyon1.fr; Fax: +33-(0)4 72-44-53-99; Tel: +33-(0)4 72-44-53-36*

[b] *Groupe d'Etudes de Métallurgie Physique et de Physique des Matériaux, (CNRS UMR 5510), INSA de Lyon, 69621, Villeurbanne cedex, France*

Received (in Strasbourg, France) 22nd January 2002, Accepted 26th April 2002
First published as an Advance Article on the web 15th August 2002

$NiRh_2S_4$ unsupported catalysts were prepared by a coprecipitation method and characterized by X-ray diffraction (XRD), chemical analysis, specific surface area measurements and high-resolution transmission electron microscopy (HRTEM). It has been shown by XRD and HRTEM that the main phase of the prepared solids has a cubic spinel type structure. The catalytic properties were evaluated in the hydrodesulfurization (HDS) of thiophene and the hydrogenation (HYD) of tetralin. The intrinsic HDS and HYD activities of the $NiRh_2S_4$ catalyst were compared with dispersed Rh, Mo binary sulfides and ternary NiMoS and $NiCr_2S_4$ sulfides. The intrinsic HDS activity of $NiRh_2S_4$ is higher than the sum of those of the individual Ni_3S_2 and Rh_2S_3 compounds, suggesting the existence of a synergistic effect between Ni and Rh.

In the field of the hydrotreatment of petroleum feedstock by sulfide catalysts, the development of preparation methods of new highly dispersed sulfides is important to progress in the understanding of the nature of the catalytic function of such systems. For instance, the synthesis of poorly crystalline V, Mo, W sulfides from thiosalt decomposition[1] or by reacting a precursor salt with Na_2S[2] or flowing H_2S was crucial for establishing the periodic trends in the catalytic activities of transition metal sulfides.[3,4] Highly dispersed Ru, Rh, Os, Ir, or Re sulfides were found to be the most active among unsupported binary systems and, by consequence, new catalytic formulations based on supported Ru sulfide have been proposed.[5]

In the industrial sulfide catalysts, the key phenomenon is the synergetic effect, observed in the so-called "CoMoS" species, where both transition metals are associated in one phase. Although many studies were devoted to the association of a transition metal sulfide dopant with Mo (W) sulfides, the synergetic effects of ternary transition metal sulfides has not yet been extensively studied. In a pyrite-type structure, Ni has been found to present a synergetic effect with RuS_2 for a hydrogenation reaction.[6]

Among ternary sulfides, a large class of compounds has the thiospinel structure. Generally formulated as AB_2S_4, these compounds mostly have the normal spinel structure, based on the sulfur close packed fcc network, in which one-eighth of the tetrahedral holes are occupied by the divalent cations A whereas half of the octahedral sites are occupied by the trivalent cations B.[7] Many studies on the electrical and magnetic properties of thiospinels have been reported[8–10] in the past and in the last years new phenomena such as spin glass,[11] magnetoresistance[12] or incommensurate structures[13] were discovered in such compounds. The catalytic properties of thiospinels have only recently been investigated: the catalytic activities of compounds containing 3d transition metals (Mn, Fe, Co, Ni, Cu, Zn) as the A ions and chromium as the B ion were examined for the hydrodesulfurization of thiophene and the hydogenation of tetralin.[14,15] In the sequence of MCr_2S_4 compounds, the most remarkable synergistic effects and the highest activities were observed for the $NiCr_2S_4$ catalyst.

As mentioned above, Rh sulfide presents excellent hydrotreating properties and the ternary thiospinel $NiRh_2S_4$ has been reported in the literature.[16] Therefore, in the present study, we prepared $NiRh_2S_4$ dispersions and studied their catalytic properties. HRTEM was also used to elucidate the detailed morphology of the $NiRh_2S_4$ particles.

Experimental

Preparation

To prepare the catalysts we used the precipitation of mixed hydrated oxides followed by sulfidation. For the preparation of the $NiRh_2S_4$ catalyst, $Ni(NO_3)_2{\cdot}6H_2O$, $RhCl_3{\cdot}2H_2O$, and $Rh(NO_3)_3{\cdot}2H_2O$ were used as precursor salts. The appropriate amounts of metal salts were first dissolved in distilled water. Then, the mixed aqueous solutions were precipitated with an excess of ammonium hydroxide (14.8 mol dm^{-3}). The coprecipitates were kept at room temperature overnight. Then, they were filtered, thoroughly washed with distilled water, dried in air at 393 K overnight and then ground in an agate mortar. In the case of coprecipitates prepared from mixed aqueous solutions containing chloride ions, the coprecipitates were first washed with ammonium nitrate (0.05 mol dm^{-3}) and then washed further with distilled water. For comparison, a $NiCr_2S_4$ sample was also prepared by the same method using $Cr(NO_3)_3{\cdot}9H_2O$ as the precursor salt. The hydrated oxides obtained were sulfided in a flow micro-reactor at 873–1073 K for 2 h in a 15% H_2S–85% N_2 mixture (4 dm^3 h^{-1}) under atmospheric pressure. After sulfidation the samples

† On leave from National Institute of Advanced Industrial Science and Technology (AIST), Tsukuba Central 5, Tsukuba 305-8565, Japan.

 DOI: 10.1039/b200914p

were cooled to room temperature under the same atmosphere and stored in sealed bottles under argon.

Characterization

X-Ray diffraction (XRD) patterns of the catalysts were recorded on a SIEMENS D500 diffractometer using Ni-filtered Cu-Kα radiation. Silicon powder was employed as an internal standard. The sample was placed on a sample holder for the XRD measurement and covered with a polyimide film, in order to preserve the sample from oxidation. The lattice parameter of the cubic spinel structure was calculated according to the least squares analysis method. The chemical composition of $NiRh_2S_4$ was determined by inductively coupled plasma spectrometry, after the sample was dissolved in *aqua regia*. Specific surface areas of the catalysts before and after the catalytic tests were measured by the BET method using nitrogen adsorption. Prior to BET measurements, the samples were outgassed at 673 K for 2 h.

Catalytic tests

Hydrodesulfurization (HDS) of thiophene was carried out in the vapor phase using a fixed-bed continuous-flow micro-reactor under atmospheric pressure. Partial pressures of hydrogen and thiophene were 9.8×10^4 and 2.9×10^3 Pa, respectively, and the total flow rate was 50 cm^3 min^{-1}. About 0.1 g of a catalyst was employed. The reaction was carried out at 573 K for more than 16 h to obtain a steady-state activity.

Hydrogenation (HYD) of tetralin in the presence of hydrogen sulfide was also carried out in the vapor phase and under high pressure, using a continuous-flow micro-reactor. Partial pressures of hydrogen, hydrogen sulfide, and tetralin were 4.5×10^6, 7.5×10^4, and 6.0×10^3 Pa, respectively, and the total flow rate was 300 cm^3 min^{-1}. The catalyst charge was also about 0.1 g. The reaction was carried out at 573 K for more than 16 h, and then the temperature was changed to be in the range 530–590 K. The HDS and HYD experiments were performed at conversions below 10% and the rates were calculated assuming a differential reactor.

Transmission electron microscopy

High-resolution transmission electron microscopy (HRTEM) was performed with a 200 kV JEOL 2010 microscope, with a point-to-point resolution of 0.195 nm (coefficient of spherical aberration $C_s = 0.5$ mm), and equipped with an EDS X-ray analyzer LINK-ISIS. Freshly sulfided samples were ground under an inert atmosphere and were ultrasonically dispersed in ethanol. The suspension was collected on carbon-coated grids. HRTEM image simulations were performed using the multislice approach developed in the Simply[17] package.

Results and discussion

Structural and textural properties

Fig. 1 shows the XRD patterns of $NiRh_2S_4$ catalyst prepared from $RhCl_3$ or $Rh(NO_3)_3$ and sulfided at different temperatures. The rise in the background below $2\theta = 35°$ was due to the presence of the polyimide film. Crystallographic identification and specific surface areas measured before the catalytic tests are summarized in Table 1. The XRD patterns show reflections corresponding to the unindexed JCPDS file of $NiRh_2S_4$ (29-0591) and resemble that of $CuRh_2S_4$ (JCPDS 17-0644), and therefore could be identified as a cubic spinel structure. The lattice constant of $NiRh_2S_4$ prepared from $RhCl_3$ was determined to be 0.967 nm and the specific surface area equal to 26 m^2 g^{-1}. Small amounts of impurities such as Rh_2S_3 and RhS_2 and/or NiS_2 (both having the same pyrite structure) were also detected besides the cubic spinel phase. As shown in Fig. 1, spectrum b, the peak intensity of $NiRh_2S_4$ prepared from $Rh(NO_3)_3$ at 873 K was weaker, and the amount of the impurity phase (the pyrite phase) was larger, compared to $NiRh_2S_4$ prepared from $RhCl_3$ at the same temperature. When the sulfidation temperature was increased from 873 K to 973 K, the peak intensity of $NiRh_2S_4$ greatly increased and the pyrite phase completely disappeared, but the Rh_2S_3 phase appeared. The Rh_2S_3 phase still remained when the sulfidation temperature was further raised to 1073 K (Fig. 1, spectrum d). The surface area of the sample prepared from $Rh(NO_3)_3$ at 873 K was 34 m^2 g^{-1}, which is larger than that of $NiRh_2S_4$ prepared from $RhCl_3$ at the same temperature (26 m^2 g^{-1}). The elemental analyses showed that the atomic ratios of Ni/Rh in $NiRh_2S_4$ prepared from $RhCl_3$ and $Rh(NO_3)_3$ were 0.54 and 0.46, respectively. These values agree reasonably well with the composition expected from the loading of the starting materials.

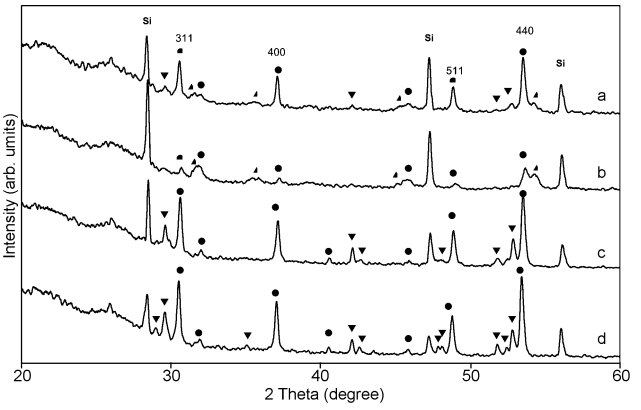

Fig. 1 XRD patterns of $NiRh_2S_4$ catalysts prepared from (*a*) $RhCl_3$ at 873 K, (*b*) $Rh(NO_3)_3$ at 873 K, (*c*) $Rh(NO_3)_3$ at 973 K, (*d*) $Rh(NO_3)_3$ at 1073 K. Labelled peaks are (●) $NiRh_2S_4$, (▼) Rh_2S_3, (▲) RhS_2 and/or NiS_2.

The HRTEM technique is helpful for characterizing solids with a small crystallographic order. In our case we obtained crystalline particles in the 10 nm size range. Even if the particles are relatively small, it is possible to get the atomic resolution images and consequently to access the crystallographic parameters. Usually, known structures are used to interpret the images with the assistance of computational techniques. We attempted to confirm that the structure of $NiRh_2S_4$ deduced from that of $CuRh_2S_4$[18] fits both diffraction pattern and atomic resolution images. For this purpose, the atomic positions of Ni and Rh were kept identical to those of Cu and Rh and S atoms moved in order to fit the cubic lattice parameter. Table 2 provides the structural data used. Two high resolution images of the same $NiRh_2S_4$ particle (composition confirmed by EDS) were obtained under different defocusing conditions (Fig. 2). At first, a FT transform (Fig. 3) was

Table 1 Crystallographic identification and specific surface areas of $NiRh_2S_4$ catalysts

Catalyst	Sulfidation temperature/K	Structure	Surface area[a] /m^2 g^{-1}
$NiRh_2S_4$(C^b)	873	$C^d + P^e + Rh_2S_3$	26
$NiRh_2S_4$(N^c)	873	C + P	34
$NiRh_2S_4$(N)	973	$C + Rh_2S_3$	11
$NiRh_2S_4$(N)	1073	$C + Rh_2S_3$	4

[a] Before the catalytic tests. [b] Prepared from $RhCl_3$. [c] Prepared from $Rh(NO_3)_3$. [d] Cubic spinel structure. [e] Pyrite structure.

Table 2 Crystallographic parameters of $NiRh_2S_4$ adapted from the $CuRh_2S_4$ cubic structure.[18] Space group *Fd*-3*m* (227), $a = 0.967$ nm

Atom	*x*	*y*	*z*
Ni	0	0	0
Rh	5/8	5/8	5/8
S	0.379	0.379	0.379

applied in order to get the zone axis and indexation of diffraction spots according to the proposed structure and a good fitting of both distances and angles was obtained. Then, the atomic resolution details observed were compared to the simulated images. Fig. 4 provides the projected potential of $NiRh_2S_4$ in the [112] direction. The electron microscope in phase contrast mode at optimum focus (Scherzer focus) should directly reveal this potential, that is the structure of the crystallite, provided the object is very thin and atom columns sufficiently separated. Once focusing is changed, the contrast-transfer function of the microscope varies and consequently images are modified.[19] The two selected pictures illustrate this effect. Black dots are transformed into white dots from one picture to another. For each picture an average atomic resolution pattern was extracted and used for matching with the computed one (Fig. 5). Simulated thickness-defocus tables (Fig. 6) were then obtained for the $NiRh_2S_4$ structure and a quantitative matching procedure was used to get a more accurate confidence level between experimental and simulated images. The resulting matches correspond to 3 and 2.5 nm for the thickness and 425 and 875 nm for the defocusing, respectively. These results support our structural assumptions (*i.e.* isostructural to $CuRh_2S_4$, and S atom shift fo fit with *a* parameter) for the $NiRh_2S_4$ compound.

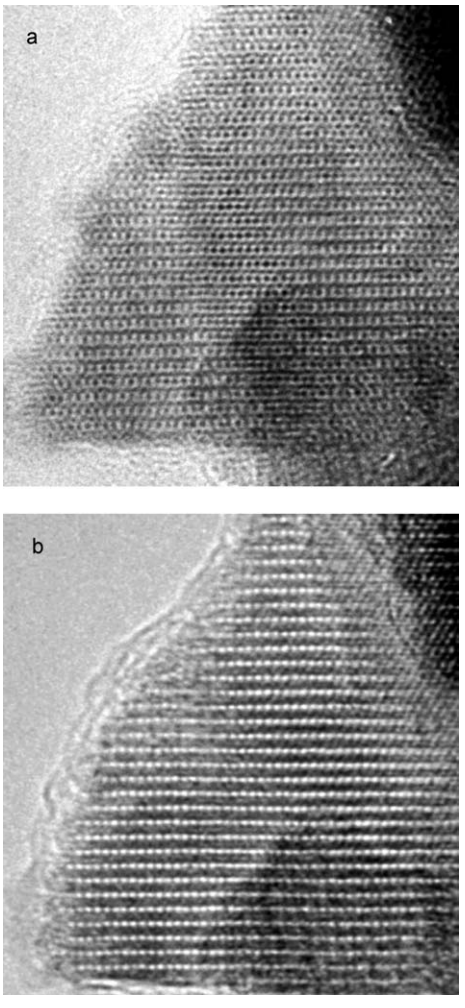

Fig. 2 HRTEM image of a $NiRh_2S_4$ particles under two different defocusing conditions.

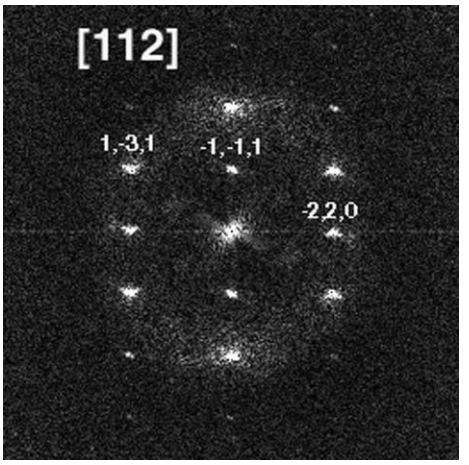

Fig. 3 Indexed Fourier transform of the HRTEM image in Fig. 2(a).

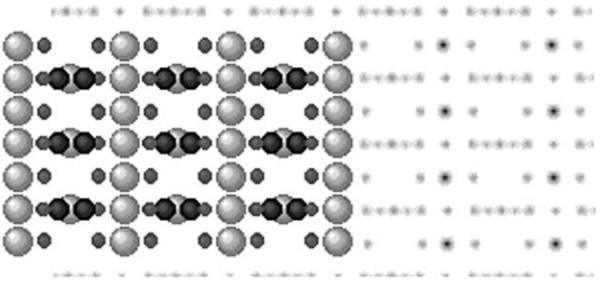

Fig. 4 Calculated projected potential of $NiRh_2S_4$ in the [112] direction.

Catalytic activity

Table 3 gives the intrinsic activities (rate per surface area) of the $NiRh_2S_4$ series of catalysts for thiophene HDS and tetralin

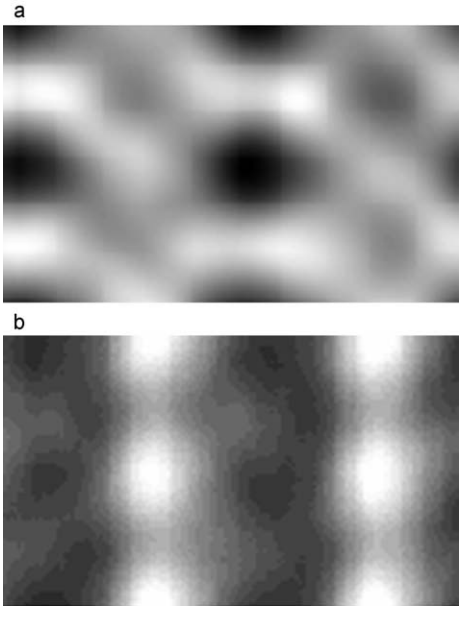

Fig. 5 Average atomic resolution pattern obtained from the HRTEM images in Fig. 2(a) and 2(b).

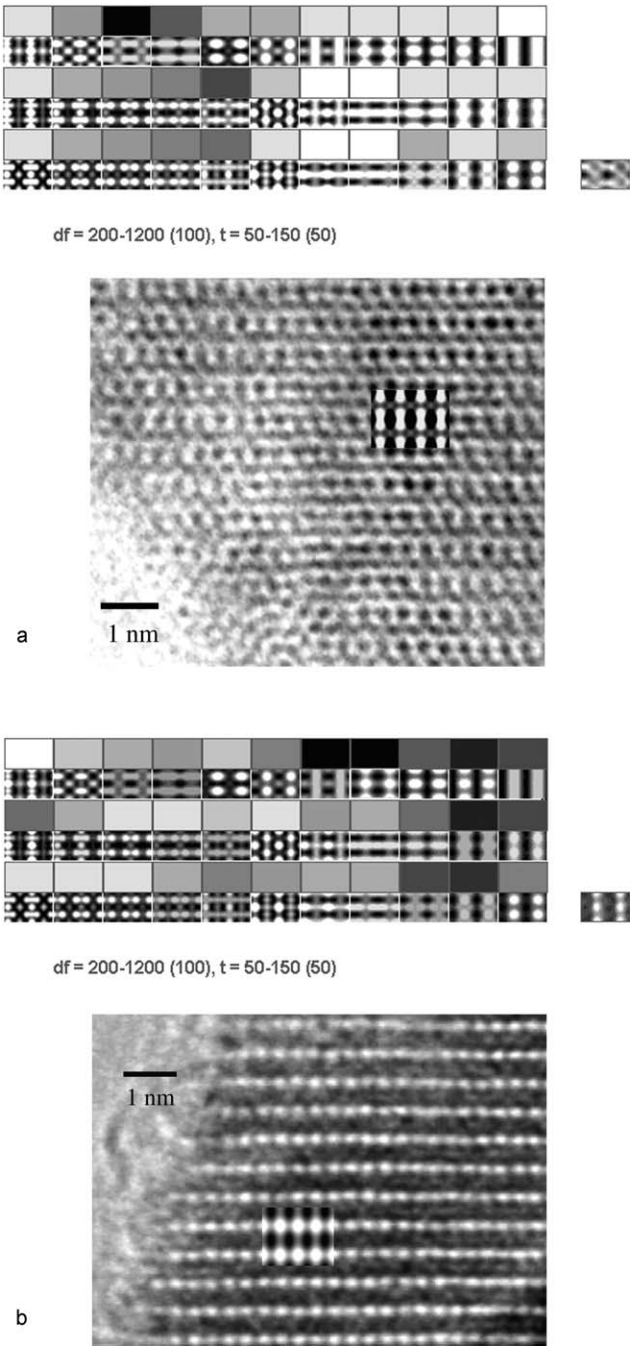

Fig. 6 Simulated thickness-defocus tables for $NiRh_2S_4$ in the [112] direction and comparison between calculated and experimental image.

HYD at 573 K. After each catalytic test, the specific surface area of the samples as well as the XRD pattern were comparable to that of the fresh sample, indicating good stability of the phase under a reducing atmosphere. Fig. 7 shows that an activation period is observed before reaching a steady state, which can be attributed to the genesis of the sulfur vacancies. Both HDS and HYD activities of $NiRh_2S_4$ prepared from $Rh(NO_3)_3$ at 873 K are higher than those of the $RhCl_3$ derived sample at the same temperature. The intrinsic catalytic activities of $NiRh_2S_4$ prepared from $Rh(NO_3)_3$ decrease with an increase in the sulfidation temperature, suggesting that sintering modifies also the nature of the catalytic sites. These catalytic activities are also compared to those of unsupported binary and ternary sulfide catalysts in Table 3. The $NiRh_2S_4$ catalysts are more active than MoS_2, and Ni_3S_2, comparable to NiMoS, Rh_2S_3, and RuS_2, but less active than $Ni_{0.6}Ru_{0.4}S_2$. Note that NiS or NiS_2 are transformed during the catalytic test

Table 3 Comparison of the intrinsic activities for the HDS of thiophene and the HYD of tetralin over various unsupported sulfide catalysts

Catalyst	Sulfidation temperature/K	Surface area/ $m^2\ g^{-1}$	Intrinsic activity at 573 K/10^{-8} mol m^{-2} s^{-1}	
			HDS	HYD
$NiCr_2S_4$	873	7	1.7	2.5
$NiRh_2S_4$ (C^a)	873	26	2.4	3.2
$NiRh_2S_4$ (N^b)	873	34	5.8	6.3
	973	11	4.2	2.6
	1073	4	2.2	
MoS_2[c]	673	18	0.31	0.83[e]
Ni_3S_2	673	6	0.74	
NiMoS[c]	673	23	3.2	1.5[e]
Rh_2S_3[d]	673	45	3.6	
RuS_2[c]	673	38	4	
$Ni_{0.6}Ru_{0.4}S_2$[c]	673	39	7.4	

[a] Prepared from $RhCl_3$. [b] Prepared from $Rh(NO_3)_3$. [c] Cited from ref. 6. [d] Calculated from reported data[10] assuming an activation energy of 67 kJ mol^{-1}. [e] Cited from ref. 21.

to Ni_3S_2, which is the stable form under the reducing conditions of the test. One can also compare the catalytic activities with that of $NiCr_2S_4$, which has a monoclinic structure and was found to be the most active compound in the series of MCr_2S_4 unsupported catalysts.[14,15] The intrinsic HDS (and HYD) activity of $NiRh_2S_4$ catalyst prepared from $Rh(NO_3)_3$ is about three times higher than that of $NiCr_2S_4$ catalyst under similar conditions[14] (Fig. 8). As compared to the NiMoS system, the synergetic effect is almost the same but $NiRh_2S_4$ is more active than NiMoS. Such a property must be related to the bond strength of M–S bonds (M = Ni, Rh) which is responsible for the catalytic activity of transition metal sulfides in hydrodesulfurization reactions.[20] In fact, DFT calculations will be helpful for another confirmation of the crystal structure of $NiRh_2S_4$ and estimation of the metal-sulfur bond strength and consequently its catalytic properties as compared to simple or mixed transition metal sulfides.

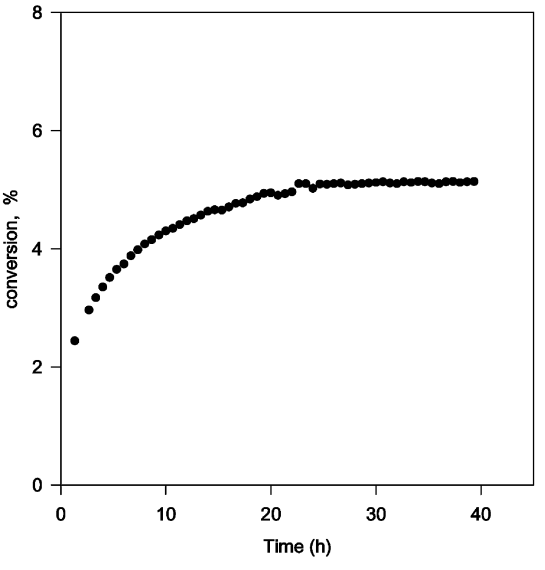

Fig. 7 Catalytic conversion of thiophene at 573 K *vs.* time for $NiRh_2S_4$ (N) catalyst.

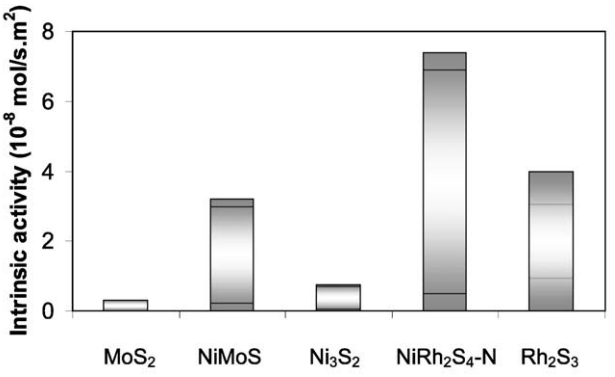

Fig. 8 Intrinsic catalytic activities in thiophene conversion for binary and ternary transition metal sulfides.

Conclusion

Dispersed unsupported ternary sulfide $NiRh_2S_4$ has been prepared by coprecipitation of precursor salts and further sulfidation. The samples obtained present relatively high surface areas. HRTEM allowed us to get a structural and morphological description of the $NiRh_2S_4$ particles. The ternary compound sulfided at 873 K and prepared from a nitrate precursor presents an intrinsic activity in HDS higher than the sum of the individual Ni_3S_2 and Rh_2S_3 compounds, implying the existence of a synergetic effect between Ni and Rh. As compared to Cr based (or derived) thiospinels or unsupported Co(Ni)Mo sulfides, $NiRh_2S_4$ presents the highest activity.

Acknowledgements

This work was carried out in the framework of the program Japan-France PICS N° 629 "Catalyst Design Concept for Environmental Issues-Characterization and Hydrogenation Activity of Non-conventional Sulfide Catalysts". H.Y. thanks the program for financial support. H.Y. also thanks Dr. A. Thiollier for experimental help.

References

1 E. Diemann and A. Müller, *Coord. Chem. Rev.*, 1973, **10**, 79.
2 R. R. Chianelli and M. B. Dines, *Inorg. Chem.*, 1978, **17**, 2758.
3 T. A. Pecoraro and R. R. Chianelli, *J. Catal.*, 1981, **67**, 430.
4 M. Lacroix, N. Boutarfa, C. Guillard, M. Vrinat and M. Breysse, *J. Catal.*, 1989, **120**, 473.
5 M. Breysse, C. Geantet, M. Lacroix, J. L. Portefaix and M. Vrinat, in *Hydrotreating Technology for Pollution Control*, eds. M. L. Ocelli and R. Chianelli, Marcel Dekker, New York, 1996, p. 169.
6 J. A. De Los Reyes, M. Vrinat, C. Geantet, M. Breysse and J. Grimblot, *J. Catal.*, 1993, **142**, 455.
7 A. Wold and K. Dwight, in *Solid State Chemistry: Synthesis, Structure and Properties of Selected Oxides and Sulphides*, Chapman and Hall, New York, 1993, ch. 11.
8 (*a*) F. K. Lotgering, *Philips Res. Rept.*, 1956, **11**, 218; (*b*) F. K. Lotgering, *Philips Res. Rept.*, 1956, **11**, 337.
9 P. K. Baltzer, P. J. Wojtowicz, M. Robbins and E. Lopatin, *Phys. Rev.*, 1966, **151**, 367.
10 J. B. Goodenough, *J. Phys. Chem. Solids*, 1969, **30**, 261.
11 S. Pouget and M. Alba, *J. Phys.: Condens. Matter*, 1995, **7**, 4739.
12 A. P. Ramirez, R. J. Cava and J. Krajewski, *Nature*, 1997, **386**, 156.
13 A. Lafond, L. Cario, A. van der Lee and A. Meerschaut, *J. Solid State Chem.*, 1996, **127**, 295.
14 A. Thiollier, P. Afanasiev, P. Delichere and M. Vrinat, *J. Catal.*, 2001, **197**, 58.
15 P. Afanasiev, A. Thiollier, P. Delichere and M. Vrinat, *Stud. Surf. Sci. Catal.*, 2000, **130**, 473.
16 K. Koerts, *Recl. Trav. Chim. Pays Bas*, 1963, **82**, 1099.
17 T. Epicier and M. A. O'Keefe, in *Proceedings 11th European Congress on Electron Microscopy EUREM 96*, CESM, Brussels, 1998, vol. 1, p. 410.
18 E. Riedel, J. Pickardt and J. Soechtig, *Z. Anorg. Allg. Chem.*, 1976, **419**, 63.
19 P. Buseck, J. Cowley and L. Eyring, *High Resolution Transmission Electron Microscopy and Associated Techniques*, Oxford University Press, Oxford, 1992.
20 H. Toulhoat, P. Raybaud, S. Kasztelan, G. Kresse and J. Hafner, *Catal. Today*, 1999, **50**, 629.
21 C. Thomazeau, Ph.D. Thesis, University of Lyon, 2001.